



Technical Note

# Geomorphological and Spatial Characteristics of Underwater Volcanoes in the Easternmost Australian-Antarctic Ridge

Hakkyum Choi <sup>1,\*</sup>, Seung-Sep Kim <sup>2</sup>, Sung-Hyun Park <sup>1</sup> and Hyoung Jun Kim <sup>3</sup>

<sup>1</sup> Division of Earth Sciences, Korea Polar Research Institute, 26 Songdomirae-ro, Yeosu-gu, Incheon 21990, Korea; shpark314@kopri.re.kr

<sup>2</sup> Department of Geological Sciences, Chungnam National University, 99 Daehak-ro, Yuseong-gu, Daejeon 34134, Korea; seungsep@cnu.ac.kr

<sup>3</sup> Office of Technology Development and Service, Korea Polar Research Institute, 26 Songdomirae-ro, Yeosu-gu, Incheon 21990, Korea; jun7100@kopri.re.kr

\* Correspondence: hkchoi@kopri.re.kr

**Abstract:** Underwater volcanoes and their linear distribution on the flanks of mid-ocean ridges are common submarine topographic structures at intermediate- and fast-spreading systems, where sufficient melt supplies are often available. Such magma sources beneath the seafloor located within a few kilometers of the corresponding ridge-axis tend to concentrate toward the axis during the upwelling process and contribute to seafloor formation. As a result, seamounts on the flanks of the ridge axis are formed at a distance from the spreading axis and distributed asymmetrically about the axis. In this study, we examined three linearly aligned seamount chains on the flanks of the KR1 ridge, which is the easternmost and longest Australian-Antarctic Ridge (AAR) segment. The AAR is an intermediate-spreading rate system located between the Southeast Indian Ridge and Macquarie Triple Junction of the Australian-Antarctic-Pacific plates. By inspecting the high-resolution shipboard multi-beam bathymetric data newly acquired in the study area, we detected 20 individual seamounts. The volcanic lineament runs parallel to the spreading direction of the KR1 segment. The geomorphologic parameters of height, basal area, volume, and summit types of the identified seamounts were individually measured. We also investigated the spatial distribution of the seamounts along the KR1 segment, which exhibits large variations in axial morphology with depth along the ridge axis. Based on the geomorphology and spatial distribution, all the KR1 seamounts can be divided into two groups: the subset seamounts of volcanic chains distributed along the KR1 segment characterized by high elevation and large volume, and the small seamounts distributed mostly on the western KR1. The differences in the volumetric magnitude of volcanic eruptions on the seafloor and the distance from the given axis between these two groups indicate the presence of magma sources with different origins.

**Keywords:** Australian-Antarctic Ridge; seamounts; underwater volcanism; multi-beam bathymetry; geomorphology



**Citation:** Choi, H.; Kim, S.-S.; Park, S.-H.; Kim, H.J. Geomorphological and Spatial Characteristics of Underwater Volcanoes in the Easternmost Australian-Antarctic Ridge. *Remote Sens.* **2021**, *13*, 997. <https://doi.org/10.3390/rs13050997>

Academic Editor: Athanassios Ganas

Received: 12 January 2021

Accepted: 2 March 2021

Published: 5 March 2021

**Publisher's Note:** MDPI stays neutral with regard to jurisdictional claims in published maps and institutional affiliations.



**Copyright:** © 2021 by the authors. Licensee MDPI, Basel, Switzerland. This article is an open access article distributed under the terms and conditions of the Creative Commons Attribution (CC BY) license (<https://creativecommons.org/licenses/by/4.0/>).

## 1. Introduction

Underwater volcanoes are the result of interaction between constructive and destructive forces during submarine volcanic eruptions [1]. Off-axis seamounts are active or extinct underwater volcanoes commonly observed on the flank of intermediate- and fast-spreading ridge systems, where sufficient magma sources are often available beneath the spreading seafloor to construct such topographic features [2–5]. Previous studies demonstrated that the melt source located close to the axis (e.g., within approximately 5 km of the axis) prefers to migrate toward the axis and hence eventually contributes to seafloor spreading rather than seamount construction [2–4,6–8].

Seamount generation occurs a few kilometers away from the axis and is asymmetrically distributed around the corresponding ridge axis because the melt source cannot

equally supply both flanks. Small seamounts (approximately <1.0 km height) near the spreading ridges are mostly associated with axial mantle upwelling under a steady-state process and lithospheric extension or cracking involving seafloor spreading [4–6], whereas seamount chains constructed by off-axis magmatism are more often related to anomalous melting in the asthenosphere and small-scale volcanic eruptions induced by fertile mantle heterogeneities [7,9–12]. Off-axis seamounts, newly found in the Australian-Antarctic Ridge (AAR), have not been fully studied for their origin and related formation processes. In this study, thus, we examined the shipboard bathymetry data to characterize the off-axis seamounts present in the AAR and investigated the causal relationships between the geomorphological characteristics and seamount formation processes.

The AAR extends eastward from the Southeast Indian Ridge (Figure 1). Due to the typically rough sea states and geographical remoteness of the study area, systematic surveys equipped with modern high-resolution technologies were not conducted until 2010 (Figure 1) [13,14]. During the last decade, marine expeditions led by Korean researchers using the R/VIB *Araon* have been conducted in the AAR system [13–15]. The spreading system of the AAR is segmented as KR1, KR2, KR3, and KR4 in the orders of distance from the Macquarie Triple Junction of the Australian-Antarctic-Pacific plates: KR1 is the closest to the Macquarie Triple Junction [13,14] (inset map in Figure 1). Among these segments of the AAR system, we investigated the seamounts near the KR1 segment, which has the highest shipboard bathymetric data coverage (Figure 1b).

Based on the shipboard magnetic data, the full spreading rates of KR1 were determined as 60–67 mm/year [13,16]. The classification scheme for global ridge systems defines an intermediate-spreading ridge as a full-spreading ridge at 50–80 mm/year [17,18]. Thus, KR1 is an intermediate-spreading ridge, implying that the study area may show variations in magma sources and crustal thickness and hence host tectonic environments favorable for seamount formation.

As the easternmost and longest segment of the AAR, the KR1 segment exhibits a series of linear seamount chains observable from the satellite-derived free-air gravity data (version 23.1) [19]. Volcanic structures are denser than the surrounding seawater and hence produce positive free-air gravity anomalies, maximized at the center of the seamounts. If the seamounts are sizable enough to induce lithospheric flexure beneath them, the negative side-lobes of free-air gravity anomalies become evident around the seamounts and their associated lineaments (Figure 1a) [20,21]. Our new high-resolution bathymetric data acquired from the KR1 segment consistently show that the three volcanic seamount chains (SC-1 in the eastern KR1, SC-2 in the central KR1, and SC-3 in the western KR1) are aligned roughly perpendicular to the KR1 ridge axis, whereas relatively small and isolated seamounts are present near the axial plateau of the western KR1 (Figure 1b). Thus, we investigated the seamount formation process in the KR1 segment of the AAR by characterizing the spatial distribution and geomorphological parameters including height, basal area at reference depth, volume, and summit type of the seamounts newly constrained by the shipboard multi-beam bathymetric data.

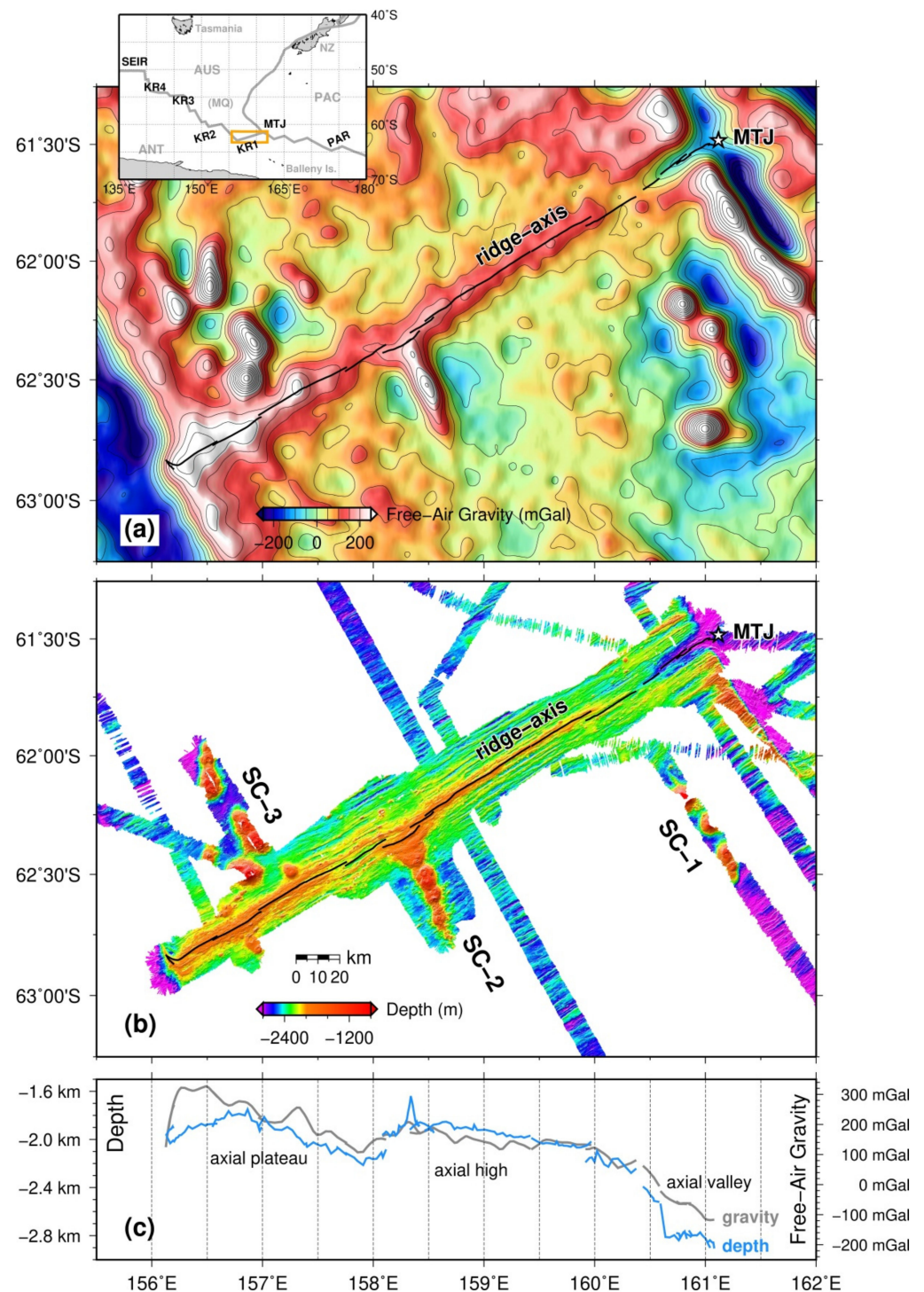


**Figure 1.** (a) Satellite-derived free-air gravity map of KR1, with a contour interval of 50 mGal (version 23.1) [19]. The spreading axis of KR1, the easternmost segment of the Australian-Antarctic Ridge (AAR), is illustrated by black solid lines. Major tectonic structures near KR1 are shown in the inset map: AUS = Australian Plate; ANT = Antarctic Plate; PAC = Pacific Plate; MQ = Macquarie Plate; SEIR = Southeast Indian Ridge; PAR = Pacific-Antarctic Ridge; MTJ = Macquarie Triple Junction; NZ = New Zealand; (b) high-resolution bathymetric map of the study area; (c) variations in depth and gravity along the ridge-axis of KR1. Blue lines show the seafloor depth from the observed multi-beam data, whereas gray lines show the free-air gravity anomalies derived from the satellite altimetry data (version 23.1) [19].

## 2. Data and Method

The first geophysical mapping, which focused on the seamount chain extending from the central ridge axis to the southeast, was conducted in early 2013 [22], and additional geophysical mapping was conducted in early 2017 to investigate the seamount volcanism in other regions on the flanks of KR1 (Figure 1b). All the survey tracks for mapping seamounts in the study area were designed to be parallel to the spreading direction of the KR1 segment, which roughly coincides with the lineament of the seamount chains near the given axis.

The high-resolution bathymetric data were collected using the multi-beam echo-sounder EM122 (Kongsberg Gruppen, Kongsberg, Norway), which has an operating frequency of 12 kHz, a depth range of 20–11,000 m, a swath width of 6 times the given depth, and a maximum of 432 soundings per swath. Raw bathymetric data were corrected based on the ship's position and attitude and gridded after manual post-processing (e.g., removal of random errors caused by the ship's motion at sea) using Teledyne CARIS (Canada).

In this study, a seamount is defined as an isolated volcanic structure that rises more than 100 m above the surrounding seafloor [20]. Seamounts tend to coalesce into a chain with topographic distinction from the seafloor (i.e., heights) [23]. Processed bathymetric data were used to identify such isolated seamounts and estimate the basal area, volume, and elevation of the identified seamounts. To estimate the geometric parameters of each volcanic edifice, we individually set a reference depth (Table 1) using the observed bathymetry data. The reference depth is the base level at which that the topography starts to rise above the seafloor. Thus, the basal area of a seamount is estimated at the reference depth, and its volume is integrated from the reference depth. To extract the coordinates of the reference depth, we used the *grdcontour* program in GMT (Generic Mapping Tools) on gridded bathymetric data [24]. However, such single and fixed reference depths estimated for individual volcanic bodies do not reflect the cooling effect of the oceanic lithosphere [25], which deepens the seafloor farther away from the ridge axis. As a result, the geometric parameters estimated with a fixed reference depth would underestimate the actual geometry of seamounts.

Due to the rough sea conditions and limited ship time, complete geophysical mapping for the seafloor domain populated with the seamounts of interest could not be obtained (e.g., seamount chain SC-1 in Figure 1b). The seamounts with incomplete bathymetry coverage were complemented with the global satellite-derived bathymetric data (version 18.1) [26] using the *grdblend* program in GMT, which merges the listed gridded data using cosine-taper weights [24]. All the shipboard bathymetric maps in this study were produced using gridded data of 50 m resolution. For merging the shipboard data with the satellite-derived data, 100 m resolution datasets were used. Then, the *grdvolume* program in GMT was applied to the original grids of 50 m resolution and, if needed, the blended grids of 100 m resolution, to calculate the basal area and the volume of the seamounts. We used GMT software to produce all the figures in this study [24].

Each seamount has one or multiple peaks with different morphological types. To characterize such morphological properties, the seamount summits were categorized as crater/caldera (c), peak (p), and flat top (f). Craters with a relatively regular circle-shaped summit can be distinguished from calderas with an irregular shape in summit morphology due to collapse. However, in this study, we are only interested in the volumetric variations of the seamounts and hence did not separate craters and calderas by summit type. The representative summit for each seamount was determined by the highest or the most voluminous morphology (marked with an asterisk in Figures 2–5) for approximating the location of the seamounts to calculate the depth from the sea level (or the height from the reference depth) and to compute the distance from the spreading axis of KR1.

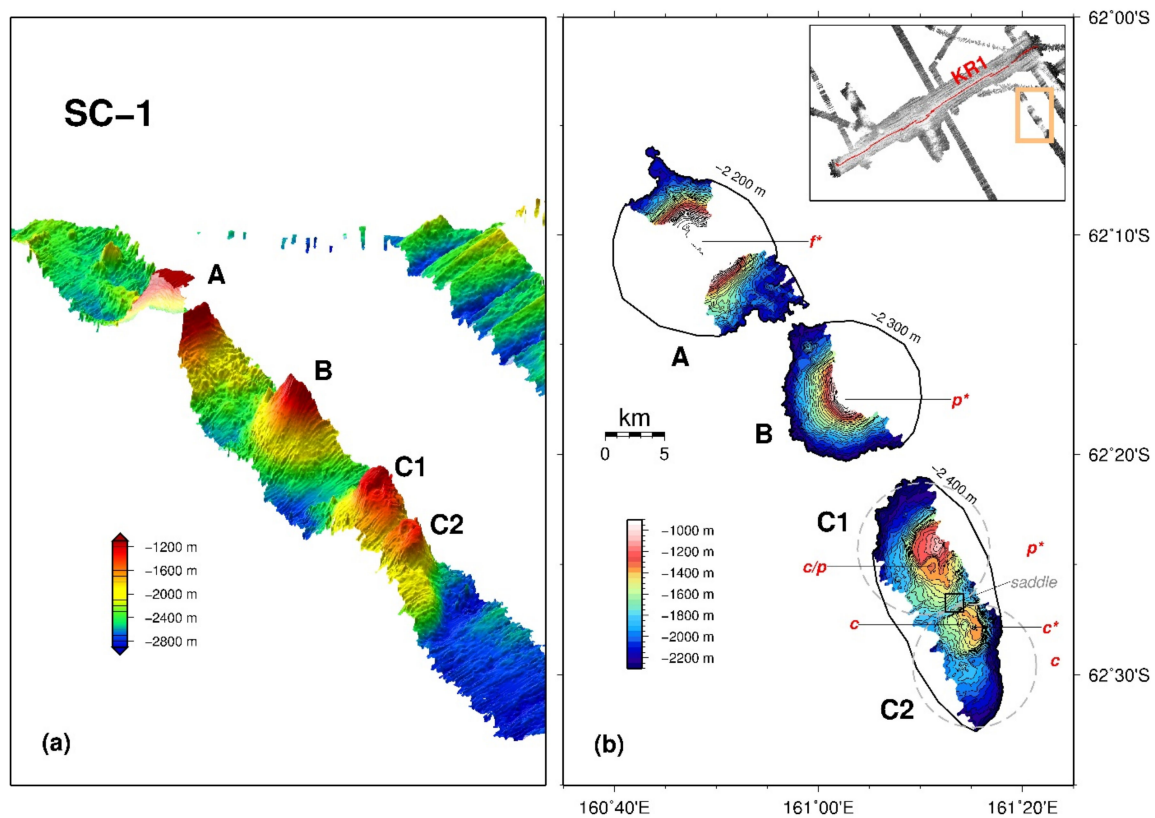


**Figure 2.** (a) 3-D perspective plot with  $5\times$  vertical exaggeration for seamount chain SC-1; (b) the geomorphological structures of isolated volcanic edifices A, B, and C (=C1 + C2) at their respective reference depths (i.e., 2200 m for seamount A; 2300 m for B; 2400 m for C), based on 50 m contoured multi-beam bathymetric data. Summit types for each seamount are marked with red letters: c = crater/caldera; p = peak; f = flat top. The letters with asterisks indicate the representative summit for each seamount.

By manually inspecting the newly acquired high-resolution multi-beam bathymetry, we identified 20 volcanic structures that protruded higher than 100 m from the surrounding seafloor. Some of the identified seamounts were grouped into three separated seamount chains based on their linear distribution. The seamounts chains were subdivided as individual summits based on a saddle structure (e.g., seamounts C1 and C2 in Figure 2). Using these identified seamounts, we conducted subsequent morphological analyses to understand the volcanic formation processes in the vicinity of the KR1 segment.

**Table 1.** List and estimated morphological parameters of the seamounts distributed on the flanks of KR1.

Name of Seamount	Reference Depth (m)	Basal Area (km <sup>2</sup> )	Volume (km <sup>3</sup> )	Summit Type <sup>1</sup>	Coordinates of Representative Summit <sup>2</sup> (Lon; Lat) [Type <sup>1</sup> ]	Height (Depth) of Representative Summit (m)	Distance from Axis to Representative Summit (km)
A	2200	~151.5	~81.5	1f	160°48.60' E; 62°10.30' S [f]	1614 (586)	54.7
B	2300	~108.2	~40.5	1p	161°02.60' E; 62°17.50' S [p]	~1400 (~900)	72.3
C	C1	~86.5	~34.5	1c, 2p	161°11.62' E; 62°24.22' S [p]	1353 (1047)	87.0
	C2	~61.3	~19.4	3c	161°15.21' E; 62°27.85' S [c]	884 (1516)	94.3

Table 1. Cont.

Name of Seamount	Reference Depth (m)	Basal Area (km <sup>2</sup> )	Volume (km <sup>3</sup> )	Summit Type <sup>1</sup>	Coordinates of Representative Summit <sup>2</sup> (Lon; Lat) [Type <sup>1</sup> ]	Height (Depth) of Representative Summit (m)	Distance from Axis to Representative Summit (km)	
D	1900	~148.5	~20.2	3c, 2p	158°23.93' E; 62°26.61' S [c]	261 (1639)	12.0	
E1		~96.9	~51.7	3c	158°28.70' E; 62°31.20' S [c]	812 (1288)	21.3	
E	E2	2100	~51.4	~23.8	2c, 1p	158°32.95' E; 62°35.95' S [p]	1170 (930)	30.8
E3			~76.9	~19.3	2c, 4p	158°35.40' E; 62°40.88' S [c]	638 (1462)	40.0
F	2100	~171.8	~92.6	1c, 1p	156°52.80' E; 62°29.88' S [c]	1412 (688)	16.4	
G	G1	2100	~127.3	~62.2	3c	156°57.05' E; 62°22.30' S [c]	1033 (1067)	26.7
G2			~100.0	~45.2	1c	156°49.55' E; 62°17.30' S [c]	939 (1161)	37.9
H	H1	2500	~208.4	~131.4	2c, 1p	156°31.60' E; 62°08.38' S [c]	1224 (1276)	60.0
H2			~82.3	~50.3	1c, 1p	156°30.60' E; 62°01.00' S [c]	841 (1659)	72.3
I	2000	~30.5	~5.0	1c, 1p	157°15.75' E; 62°29.58' S [c]	434 (1566)	6.7	
J	2200	~60.8	~10.8	1c, 1p	156°31.07' E; 62°25.22' S [c]	630(1570)	35.4	
K	2050	~30.0	~3.3	1c, 4p, 1f	156°40.28' E; 62°39.36' S [c]	258 (1792)	8.6	
L	2050	~7.5	~0.7	1p	156°46.30' E; 62°35.90' S [p]	294 (1756)	11.4	
M	2050	~3.8	~0.4	2f	156°48.73' E; 62°34.77' S [f]	192 (1858)	11.7	
N	2000	~39.4	~4.9	2c, 1p	156°57.78' E; 62°48.40' S [c]	114 (1886)	13.2	
O	2000	~4.2	~0.5	1p	156°56.45' E; 62°43.70' S [p]	314 (1686)	5.4	

<sup>1</sup> Seamount summits are classified as craters/calderas (c), peaks (p), or flat tops (f). <sup>2</sup> The representative summit of each volcanic structure is marked with an asterisk in Figures 2–5.

### 3. Results

The seamounts identified in the high-resolution multi-beam shipboard bathymetry data are distributed in three areas, on the flanks of the eastern, central, and western KR1, similar to the classification of the axial morphology of KR1 (Figure 1c). In the eastern KR1, where the valley-shaped seafloor structure has axial morphology, seamount chain SC-1 extends to the southeast at a considerable distance from the axis of seafloor spreading. Seamount chain SC-2 extends to the southeast from the axis in the central KR1, where the axial high is observed (Figure 1b). In the western KR1, where the axial plateau is observed, seamount chain SC-3, consisting of considerably large seamounts, is distributed on the northwest flank with a set of smaller seamounts populated on both flanks of the western KR1 (Figure 1b).

These seamount chains are numbered sequentially from east to west, similar to the numbering scheme for the spreading segments of the AAR. In addition, each individual seamount is named alphabetically from east to west along the ridge axis and from the nearest to the farthest on the given axis. A list of the volcanic seamounts and the measured morphological parameters are presented in Table 1.

### 3.1. Eastern KR1: SC-1

Seamount chain SC-1, which is located near the eastern end of KR1, is composed of three isolated volcanic structures A, B, and C, and extends southward. Among the discovered seamount chains in the study area, SC-1 is currently located at the most distant point from the KR1 axis (more than 40 km) and linearly distributed along a ~60 km distance (Figure 1b). Three volcanoes in SC-1 have steep slopes of  $>12^\circ$  (Figure 2 and Table 1). SC-1 seamounts A, B, and C (=C1 + C2) have a total basal area of ~410 km<sup>2</sup> and a total volume of ~180 km<sup>3</sup> at the given reference depths. The representative summits of these seamounts extend more than 1300 m above the reference depth (Table 1).

Seamount A, located at approximately 45–65 km from the ridge axis, represents a circular base at the reference depth of 2200 m and a single flat top inferred from the merged bathymetry grid. The only summit of seamount A is the highest of all the volcanoes discovered in the surveyed area of segment KR1. Its elevation extends over 1600 m above the reference depth, reaching only ~600 m below the sea surface (Figure 2 and Table 1).

Seamount B located at approximately 65–80 km from the ridge axis also has a circular-shaped base and only one summit constrained by the merged bathymetric data. The summit is estimated to be shaped as a steep peak with ~1400 m in elevation from the reference depth of 2300 m, although the summit area has not been fully surveyed by high-resolution bathymetry (Figure 2 and Table 1).

Seamount C, located approximately 80–100 km from the ridge axis, has an elongated base in the oblique direction to seafloor spreading (unlike seamounts A and B of a circular base) (Figure 2). Seamount C also consists of two volcanic structures, C1 and C2, which topographically overlap with each other. Each volcanic structure has several craters, calderas, and peaks (Figure 2 and Table 1). At the top of C1, a steep peak with an elevation of more than 1300 m from the reference depth of 2400 m appears, and a caldera collapse is observed on the southern flank of the seamount top (Figure 2 and Table 1). Similarly, several crater or caldera structures are apparent at the top of seamount C2. In addition, a significant topographic change in elevation is observed at the northwest slope connected to seamount C1 (Figure 2).

### 3.2. Central KR1: SC-2

SC-2, a seamount chain in the central section of KR1, is fully covered by multi-beam mapping along a series of survey lines. SC-2 is connected to the ridge axis; it extends to the southeast (~50 km) and features approximately two volcanic structures D and E (with three seamounts E1, E2, and E3). Although the overall height and size of the SC-2 seamounts are smaller than those of the other seamount chains (Figure 1 and Table 1), these seamounts exhibit a large number of craters/calderas and peaks constrained by shipboard bathymetry (Figure 3). The central region of KR1 is shallower than the eastern KR1 (Figure 1c), and the northern end of SC-2 is shown as a broad, elevated area at the ridge axis.

Seamount D is quite low in elevation compared with any other volcanic edifice constituting a seamount chain in KR1 (Figure 1b). The northernmost peak-type summit is located on the spreading axis, and a pattern parallel to the fabric of the spreading seafloor has the base shape at the reference depth of 1900 m (Figure 3). Higher elevation and more distinct shapes are observed at the summits of seamount D (Figure 3), farther away from the ridge axis. The highest summit of seamount D, located farthest from the axis (~12 km), represents a crater (Figure 3 and Table 1).

Seamount E is largely divided into three volcanic structures, E1, E2, and E3, based on topographical changes such as a noticeable saddle structure between volcanic edifices, and

each edifice has several summits (Figure 3). Seamounts E1 and E2 are not morphologically distinct, whereas the smaller edifice E3 is distinguished from the others. In seamount E, which is distributed linearly with a total length of ~35 km, the most prominent volcanic body is E1, which has an elevation of ~800 m and shows a large caldera collapse on the northern flank of the representative summit (Figure 3 and Table 1). Although volcanic edifice E2 has less than half the volume of E1, it represents the highest summit of ~1200 m in SC-2 (Figure 3 and Table 1).

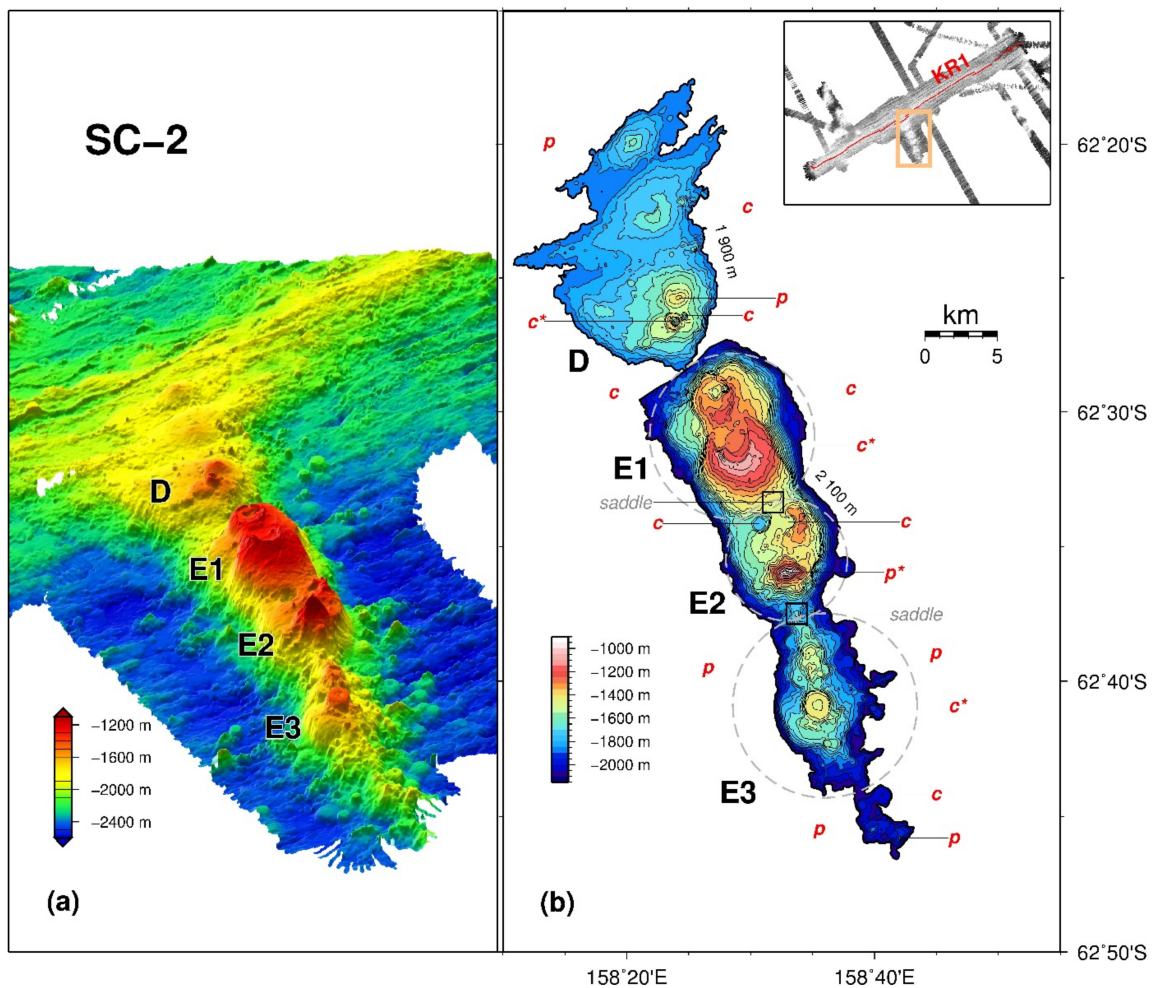


**Figure 3.** (a) 3-D perspective plot with 5x vertical exaggeration for seamount chain SC-2, which stretches to the southeast from the KR1 axis; (b) the morphological structures of seamounts D and E (=E1 + E2 + E3) from the reference depth (i.e., 1900 m for seamount D and 2100 m for E)—the bathymetric contour interval is 50 m. Summit types for each seamount are marked with red letters: c = crater/caldera; p = peak; f = flat top. Letters with asterisks indicate the representative summit for each seamount.

### 3.3. Western KR1: SC-3 and Small Seamounts

In the western section of KR1, we detected numerous volcanic structures, indicating the presence of a surplus magma supply system in the western area. This area exhibits a broad axial high and irregularly distributed seamounts (Figure 1b); five volcanic bodies, namely F, G (=G1 + G2), H (=H1 + H2), I, and J, were identified (Figure 4). These volcanic edifices, particularly F, G, and H of SC-3, have larger basal areas and volumes than other KR1 seamounts (Table 1). SC-3 with a scattered spatial distribution exhibits a roughly linear array with a length of approximately 80 km, stretching out from the ridge axis (Figure 4).

Similar to seamounts A and B in SC-1, seamount F is an independent volcanic structure that represents a high elevation of approximately 1400 m with a circular base at the reference

depth of 2100 m (Figure 4 and Table 1). A crater-type summit was observed in the center of the seamount, and a lower peak-type summit was found on the northwestern flank of the representative summit (Figure 4).

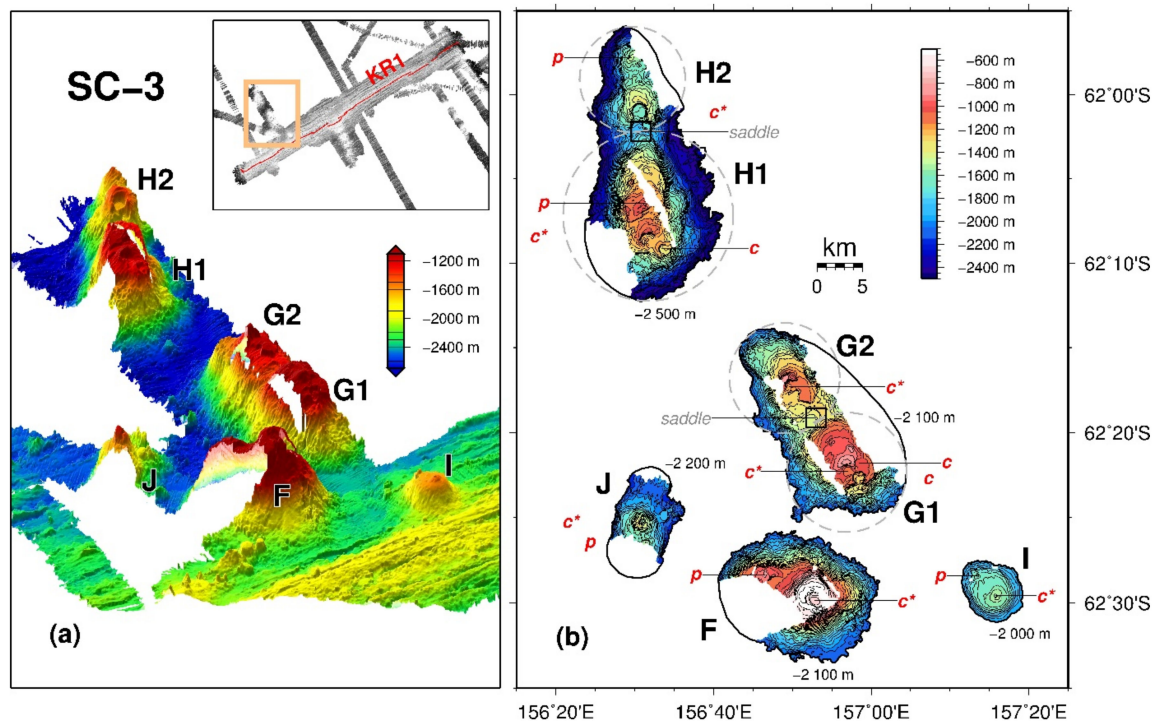


**Figure 4.** (a) A 3-D perspective plot with 5x vertical exaggeration for seamount chain SC-3; (b) detailed geomorphologies of seamounts F, G (=G1 + G2), H (=H1 + H2), I, and J from each reference depth (i.e., 2000 m for seamount F; 2100 m for G and I; 2200 m for J; 2500 m for H) with 50 m contour are represented along with the summit types of the seamounts (c = crater/caldera; p = peak; f = flat top). The letters with asterisks indicate the representative summit for each seamount.

Seamount G, representing several craters and caldera collapses, is subdivided into seamounts G1 and G2 and has a ~30 km-long feature of base in a direction substantially coincident with seafloor spreading (Figure 4). Both seamounts G1 and G2 represent a caldera-type summit with the height of ~1000 m from the reference depth of 2100 m (Table 1).

Seamount H is approximately 50–80 km away from the spreading ridge and has a linear-shaped base oblique to the seafloor spreading direction (Figure 4) at the reference depth of 2500 m. The seamount is subdivided into H1 and H2, and H1 is the largest volcanic edifice among all newly discovered KR1 seamounts, with a basal area of ~210 km<sup>2</sup> (~300 km<sup>2</sup> for the seamount H) and a volume of ~130 km<sup>3</sup> (~180 km<sup>3</sup> for H) (Table 1).

Seamount I is a small seamount with an elevation of ~400 m and a volume of only ~5 km<sup>3</sup>, showing substantial difference from the other seamounts that compose the seamount chains of KR1 (Figure 4 and Table 1). Another small seamount, J, with an elevation of ~600 m and a volume of ~10 km<sup>3</sup>, represents the crater-type summit at a distance of approximately 35 km from the ridge axis (Figure 4 and Table 1). Based on their small size, seamounts I and J can also be grouped with small volcanic seamounts K to O around the western KR1. Several small seamounts (K, L, M, N, and O) were also detected in both flanks of western KR1 (Figure 5), with elevations ≤400 m and volumes ≤5 km<sup>3</sup> (Table 1).

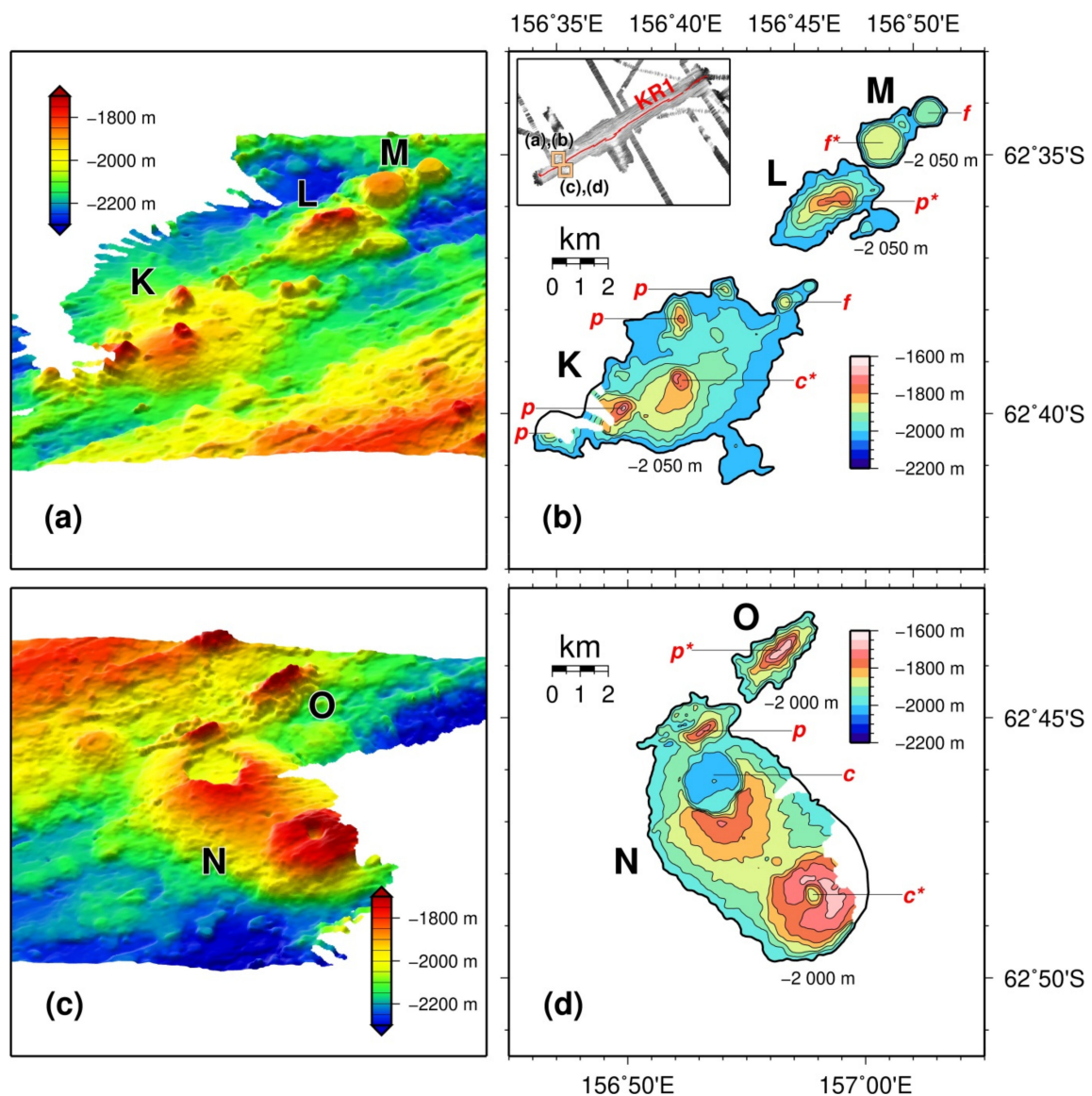


**Figure 5.** (a) Small seamounts and the seafloor, located on the northern flank of western KR1; (b) detailed morphology and distribution of seamounts K, L, and M from the reference depth (i.e., 2050 m for all); (c) the detected seafloor with small mounds on the southern flank of western KR1; (d) the morphology of seamounts N and O from the reference depth (i.e., 2000 m for both). The contour interval of bathymetry is 50 m. The letters with asterisks indicate the representative summit for each seamount.

#### 4. Discussion

The axial morphology of KR1 can be divided into the eastern section featuring the axial valley, the central section with the axial high, and the western section with numerous seamounts, and the axial plateau (Figure 1b,c) [16,24,27,28]. According to the division by axial morphology, excessive magma supply in the western section of KR1 is expected to be much higher than that in the eastern section. However, there is no apparent correlation between the ridge morphology and spatial distribution of seamounts along the ridge axis (e.g., size and volume) (Figure 6), owing to not only the presence of most voluminous seamounts in the western section but also the sizable seamounts in the eastern section (Figures 1b and 6). The eastern section likely had an excessive magma supply that allowed for the construction of large seamounts (A, B, and C), although the present ridge morphology of the rift valley implies a lack of magma supply. In other words, the presence of the identified seamounts requires an alternative option for the magma source for the given seamount construction.

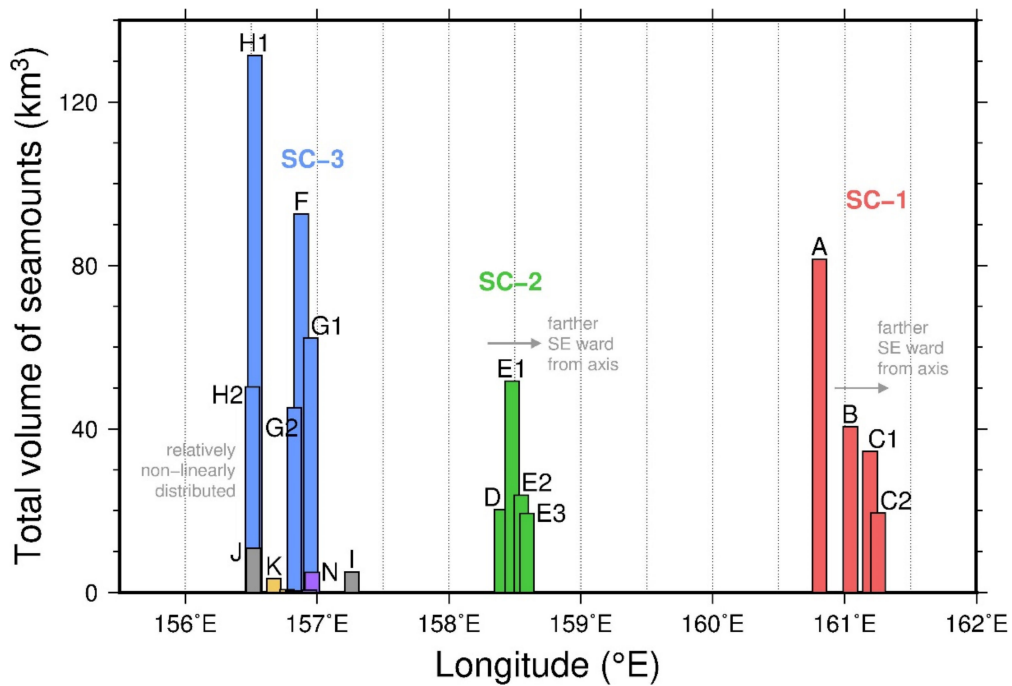


**Figure 6.** Longitudinal distribution and volume of seamounts along the KR1 segment. The major seamount chains of SC-1, SC-2, and SC-3 are shown in red, green, and blue bars, respectively, and the smaller seamounts distributed near SC-3 in the west of KR1 are marked in other colors.

Figure 7 shows the linear relationship between the basal area and the volume of the seamounts in the study area. In general, a voluminous seamount requires a wide basal area during its growing phase. However, there is a significant difference in the linear relationship between the seamounts composing the linear chains and the off-axis seamounts observed mostly in the western KR1. The group exhibiting a large basal area and volume is characterized by ~520 m height increments as the basal area increases. Another seamount group follows the linear relationship with ~150 m height increments (Figure 7).

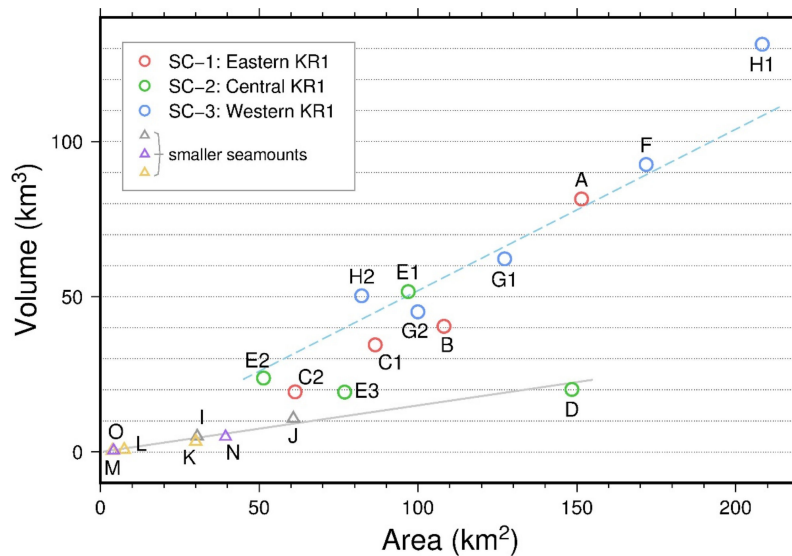


**Figure 7.** Basal area versus volume for each seamount. Seamounts can be divided into two groups by the linear relationship between their basal area and volume: a group following the trend of the dashed light-blue line and a group following the trend of the solid light-gray line.

The difference in the linear trends between the two groups can be attributed to their primitive origins. Small-scale seamounts near the spreading ridge are formed by axial mantle upwelling, related to the evolution of the oceanic lithosphere near the spreading seafloor [4–6], whereas large-scale seamount chains originate from the small-scale mantle upwelling by fertile mantle heterogeneities [9–11].

Small seamounts of the northern East Pacific Rise in the Pacific Ocean with lower than 200 m in elevation were formed at 5–15 km from the ridge axis [4,8]. The formation of small seamounts within ~10 km of the ridge implies that they have competed with the other volcanic structures for a limited magma supply. Hence, the mechanism of melt delivery to such small seamounts would not be fully mature [8]. However, the Lamont seamounts are observed at ~8 km from the northern East Pacific Rise with over 1000 m in height and forming a ~50 km long seamount chain, which originated from a heterogeneous mantle source representing depleted incompatible elements [10]. On the Juan de Fuca Ridge, located on the west coast of North America, the off-axis seamounts of over 1000 m in elevation originated from the migration of the ridge crest over a heterogeneous asthenosphere [9].

In KR1, the basalts collected from seamounts E2 and E3 in SC-2 exhibit radiogenic and isotopic enrichment [29,30], which implies that the alkalic basalts from SC-2 originate from magma with low-fractionated heavy isotopes [9]. The compositional heterogeneity in the upper mantle can facilitate melt buoyancy and a small-scale upwelling at a considerable distance from the ridge axis [7,9–12]. Our previous study on marine magnetic data acquired from the seamount chains of KR1 [16] estimated that the volcanic edifices comprising the seamount chains were largely a result of the off-axis volcanic eruptions located approximately 10–20 km from the ridge axis.

## 5. Conclusions

Seamount volcanism in KR1, the easternmost segment of the Australian-Antarctic Ridge, was characterized, and the spatial distribution, geomorphology, and types of summits were identified using multi-beam bathymetric mapping. The spatial distribution of KR1 seamounts was divided into three regions: eastern, central, and western KR1. A dominant seamount chain with a linear distribution parallel to the spreading direction of the seafloor appears in each area: SC-1 in the eastern KR1, SC-2 in the central KR1, and SC-3 in the western KR1.

A total of 20 seamounts detected in the study area have the volumes of approximately 0.5–130 km<sup>3</sup> and basal areas of approximately 4–210 km<sup>2</sup>. All the seamounts in KR1 are divided into two groups considering the magnitude of volcanoes and the distance from the ridge axis. Most seamounts comprising the seamount chains have large values of height, basal area, and volume, and they are likely originated from small-scale upwelling caused by mantle heterogeneities from the asthenosphere. The volume of seamounts in this group tends to increase by a coefficient of ~520 m in height as the basal area increases. The volume of the other group with a series of small seamounts located mostly at the western KR1 increases by a coefficient of ~150 m in height as the basal area increases, and hence the seamounts are likely associated with the axial magma upwelling near the ridge.

**Author Contributions:** Participation on cruises, data acquisition and analysis, producing map and figures, original draft preparation and editing, H.C.; Cruise design, participation on cruises, data acquisition and analysis, manuscript review and editing, S.-S.K.; Project administration, cruise design, participation on cruises, manuscript review and editing, S.-H.P.; Participation on cruises, data acquisition and analysis, H.J.K. All authors have read and agreed to the published version of the manuscript.

**Funding:** This research was supported by the Korea Polar Research Institute, grant number PE20210 and PE21050. S.-S.K. acknowledges support from the National Research Foundation of Korea (NRF) (MOE NRF-2017R1D1A1A02018632).

**Data Availability Statement:** The data presented in this study are available on request from the corresponding author. The data are not publicly available due to the presence of other ongoing studies utilizing the data.

**Acknowledgments:** We thank the captain and crews of the R/VIB *Araon* for their efforts during the scientific expeditions. We are grateful to three reviewers for their constructive comments.

**Conflicts of Interest:** The authors declare no conflict of interest.

## References

1. Casalbore, D. Volcanic Islands and Seamounts. In *Submarine Geomorphology*; Springer: Cham, Switzerland, 2017; pp. 333–347.
2. Clague, D.A.; Reynolds, J.R.; Davis, A.S. Near-ridge seamount chains in the northeastern Pacific Ocean. *J. Geophys. Res. Solid Earth* **2000**, *105*, 16541–16561. [[CrossRef](#)]
3. Coumans, J.P.; Stix, J.; Clague, D.A.; Minarik, W.G. The magmatic architecture of Taney Seamount-A, NE Pacific Ocean. *J. Petrol.* **2015**, *56*, 1037–1067. [[CrossRef](#)]
4. Scheirer, D.S.; Macdonald, K.C. Near-axis seamounts on the flanks of the East Pacific Rise, 8°N to 17°N. *J. Geophys. Res. Solid Earth* **1995**, *100*, 2239–2259. [[CrossRef](#)]
5. White, S.M.; Macdonald, K.C.; Scheirer, D.S.; Cormier, M.-H. Distribution of isolated volcanoes on the flanks of the East Pacific Rise, 15.3°S–20°S. *J. Geophys. Res. Solid Earth* **1998**, *103*, 30371–30384. [[CrossRef](#)]
6. Briais, A.; Ondréas, H.; Klingelhoefer, F.; Dosso, L.; Hamelin, C.; Guillou, H. Origin of volcanism on the flanks of the Pacific-Antarctic ridge between 41°30'S and 52°S. *Geochem. Geophys. Geosyst.* **2009**, *10*, 1–20. [[CrossRef](#)]
7. Katz, R.F.; Spiegelman, M.; Holtzman, B. The dynamics of melt and shear localization in partially molten aggregates. *Nature* **2006**, *442*, 676–679. [[CrossRef](#)]
8. Alexander, R.T.; Macdonald, K.C. Small off-axis volcanoes on the East Pacific Rise. *Earth Planet. Sci. Lett.* **1996**, *139*, 387–394. [[CrossRef](#)]
9. Davis, E.E.; Karsten, J.L. On the cause of the asymmetric distribution of seamounts about the Juan de Fuca ridge: Ridge-crest migration over a heterogeneous asthenosphere. *Earth Planet. Sci. Lett.* **1986**, *79*, 385–396. [[CrossRef](#)]
10. Fornari, D.J.; Perfit, M.R.; Allan, J.F.; Batiza, R.; Haymon, R.; Barone, A.; Ryan, W.B.F.; Smith, T.; Simkin, T.; Luckman, M.A. Geochemical and structural studies of the Lamont seamounts: Seamounts as indicators of mantle processes. *Earth Planet. Sci. Lett.* **1988**, *89*, 63–83. [[CrossRef](#)]
11. Harmon, N.; Forsyth, D.W.; Weeraratne, D.S.; Yang, Y.; Webb, S.C. Mantle heterogeneity and off axis volcanism on young Pacific lithosphere. *Earth Planet. Sci. Lett.* **2011**, *311*, 306–315. [[CrossRef](#)]
12. Wilson, D.S. Focused mantle upwelling beneath mid-ocean ridges: Evidence from seamount formation and isostatic compensation of topography. *Earth Planet. Sci. Lett.* **1992**, *113*, 41–55. [[CrossRef](#)]
13. Choi, H.; Kim, S.-S.; Dyment, J.; Granot, R.; Park, S.-H.; Hong, J.K. The kinematic evolution of the Macquarie Plate: A case study for the fragmentation of oceanic lithosphere. *Earth Planet. Sci. Lett.* **2017**, *478*, 132–142. [[CrossRef](#)]
14. Hahm, D.; Baker, E.T.; Rhee, T.S.; Won, Y.-J.; Resing, J.A.; Lupton, J.E.; Lee, W.-K.; Kim, M.; Park, S.-H. First hydrothermal discoveries on the Australian-Antarctic Ridge: Discharge sites, plume chemistry, and vent organisms. *Geochem. Geophys. Geosyst.* **2015**, *16*, 3061–3075. [[CrossRef](#)]
15. Park, S.-H.; Langmuir, C.H.; Sims, K.W.W.; Blichert-Toft, J.; Kim, S.-S.; Scott, S.R.; Lin, J.; Choi, H.; Yang, Y.-S.; Michael, P.J. An isotopically distinct Zealandia–Antarctic mantle domain in the Southern Ocean. *Nat. Geosci.* **2019**, *12*, 206–214. [[CrossRef](#)]
16. Choi, H.; Kim, S.-S.; Park, S.-H. Magnetic constraints of off-axis seamount volcanism in the easternmost segment of the Australian-Antarctic Ridge. *Geochem. Geophys. Geosyst.*. Submitted.
17. Dick, H.J.B.; Lin, J.; Schouten, H. An ultraslow-spreading class of ocean ridge. *Nature* **2003**, *426*, 405–412. [[CrossRef](#)] [[PubMed](#)]
18. Macdonald, K.C. Mid-ocean ridge tectonics, volcanism, and geomorphology. In *Encyclopedia of Ocean Sciences*; Steele, J., Thorpe, S., Turekian, K., Eds.; Academic Press: San Diego, CA, USA, 2001; pp. 1798–1813.
19. Sandwell, D.T.; Müller, R.D.; Smith, W.H.F.; Garcia, E.; Francis, R. New global marine gravity model from CryoSat-2 and Jason-1 reveals buried tectonic structure. *Science* **2014**, *346*, 65–67. [[CrossRef](#)]
20. Kim, S.-S.; Wessel, P. New global seamount census from altimetry-derived gravity data. *Geophys. J. Int.* **2011**, *186*, 615–631. [[CrossRef](#)]
21. Hwang, G.; Kim, S.-S. Flexure and gravity anomalies of the oceanic lithosphere beneath the Louisville seamount. *Tectonophysics* **2016**, *686*, 19–26. [[CrossRef](#)]
22. Choi, H.; Kim, S.-S.; Park, S.-H. Interpretation of bathymetric and magnetic data from the easternmost segment of Australian-Antarctic Ridge, 156°–161°E. In Proceedings of the AGU Fall Meeting, San Francisco, CA, USA, 9–13 December 2013. T13A-2498.
23. Rappaport, Y.; Naar, D.F.; Barton, C.C.; Hey, R.N.; Liu, Z.J. Morphology and distribution of seamounts surrounding Easter Island. *J. Geophys. Res. Solid Earth* **1997**, *102*, 24713–24728. [[CrossRef](#)]
24. Wessel, P.; Smith, W.H.F.; Scharroo, R.; Luis, J.F.; Wobbe, F. Generic mapping tools: Improved version released. *EOS Trans. Am. Geophys. Union* **2013**, *94*, 409–410. [[CrossRef](#)]

25. Parsons, B.; Sclater, J.G. An analysis of the variation of ocean floor bathymetry and heat flow with age. *J. Geophys. Res. Space Phys.* **1977**, *82*, 803–827. [[CrossRef](#)]
26. Smith, W.H.F.; Sandwell, D.T. Global sea floor topography from satellite altimetry and ship depth soundings. *Science* **1997**, *277*, 1956–1962. [[CrossRef](#)]
27. Kim, S.-S.; Lin, J.; Park, S.-H.; Choi, H. Geophysical investigation of Australian-Antarctic Ridge using high-resolution gravity and bathymetry. In Proceedings of the AGU Fall Meeting, San Francisco, CA, USA, 14–18 December 2015. DI51B-2628.
28. Park, S.-H.; Langmuir, C.H.; Lin, J.; Kim, S.-S.; Hahm, D.; Michael, P.J.; Scott, S.R.; Sims, K.W.W. Mantle domain and segmentation at the Australian-Antarctic Ridge. In Proceedings of the AGU Fall Meeting, San Francisco, CA, USA, 15–19 December 2014. OS53C-1055.
29. Yi, S.-B.; Lee, M.-J.; Park, S.-H.; Han, S.; Yang, Y.-S.; Choi, H. Occurrence of ice-rafted erratics and the petrology of the KR1 seamount trail from the Australian–Antarctic Ridge. *Int. Geol. Rev.* **2018**, *61*, 1429–1445. [[CrossRef](#)]
30. Yi, S.-B.; Lee, M.J.; Park, S.-H.; Nagao, K.; Han, S.; Yang, Y.-S.; Choi, H.; Baek, J.; Sumino, H. Alkalic to tholeiitic magmatism near a mid-ocean ridge: Petrogenesis of the KR1 Seamount Trail adjacent to the Australian-Antarctic Ridge. *Int. Geol. Rev.* **2020**, 1–21. [[CrossRef](#)]